Received: 11 September 2019 | Revised: 5 February 2020 | Accepted: 26 February 2020

DOI: 10.1002/mrm.28259

FULL PAPER

Magnetic Resonance in Medicine

Myelin water fraction estimation using small-tip fast recovery MRI

Steven T. Whitaker[1] | **Gopal Nataraj**[2] | **Jon-Fredrik Nielsen**[3] | **Jeffrey A. Fessler**[1]

[1]Department of Electrical Engineering and Computer Science, University of Michigan, Ann Arbor, MI, USA

[2]Department of Medical Physics, Memorial Sloan Kettering Cancer Center, New York, NY, USA

[3]Department of Biomedical Engineering, University of Michigan, Ann Arbor, MI, USA

Correspondence
Steven T. Whitaker, Department of Electrical Engineering and Computer Science, University of Michigan, 4125 EECS, 1301 Beal Ave, Ann Arbor, MI 48109, USA.
Email: stwhit@umich.edu

Funding information
NIH, Grant/Award Number: R21 AG061839

Purpose: To demonstrate the feasibility of an optimized set of small-tip fast recovery (STFR) MRI scans for rapidly estimating myelin water fraction (MWF) in the brain.
Methods: We optimized a set of STFR scans to minimize the Cramér-Rao Lower Bound of MWF estimates. We evaluated the RMSE of MWF estimates from the optimized scans in simulation. We compared STFR-based MWF estimates (both modeling exchange and not modeling exchange) to multi-echo spin echo (MESE)-based estimates. We used the optimized scans to acquire in vivo data from which a MWF map was estimated. We computed the STFR-based MWF estimates using PERK, a recently developed kernel regression technique, and the MESE-based MWF estimates using both regularized non-negative least squares (NNLS) and PERK.
Results: In simulation, the optimized STFR scans led to estimates of MWF with low RMSE across a range of tissue parameters and across white matter and gray matter. The STFR-based MWF estimates that modeled exchange compared well to MESE-based MWF estimates in simulation. When the optimized scans were tested in vivo, the MWF map that was estimated using a 3-compartment model with exchange was closer to the MESE-based MWF map.
Conclusions: The optimized STFR scans appear to be well suited for estimating MWF in simulation and in vivo when we model exchange in training. In this case, the STFR-based MWF estimates are close to the MESE-based estimates.

KEYWORDS
kernel ridge regression, machine learning, myelin water fraction (MWF), scan optimization, small-tip fast recovery (STFR)

1 | INTRODUCTION

Quantitative magnetic resonance imaging (QMRI) is the application of MRI to estimate parameters of interest. One QMRI application of growing interest is myelin water imaging, where one seeks quantitative maps of myelin water fraction (MWF).[1,2] The MWF is the proportion of MRI signal in a given voxel that originates from water bound within the myelin sheath. MWF maps are desirable for tracking progression of demyelinating diseases,[2] for example, multiple sclerosis.[3]

The most widely accepted myelin water imaging techniques use the multi-echo spin echo (MESE) MRI scan (or variants).[3-5] MESE is the standard for clinical MWF imaging to which alternative MWF mapping techniques are typically compared. However, MESE traditionally suffers from long scan times, impeding its routine clinical use. Alternatively, a combined gradient and spin echo (GRASE) MRI scan, a variant of MESE, has been shown to enable whole-brain MWF maps in under 8 minutes.[6]

An alternative to MESE-based myelin water imaging uses faster, steady-state MRI scans[7] that can acquire whole-brain MWF maps in 7 minutes.[6] Despite evidence showing that this method produces reproducible MWF maps (thus enabling longitudinal studies), there are concerns about overestimating the true MWF[8,9] and its precision.[10] Other steady-state methods have also been explored for MWF estimation, such as multi-echo gradient echo (GRE)[11-13] and dual-echo steady-state (DESS).[14-16]

To our knowledge, most of these myelin water imaging techniques ignore potential differences in the effective magnetic field experienced by myelin-bound water compared to water outside of myelin (an exception being[13]). However, it has been shown that in cerebral white matter (WM), myelin-bound water does in fact experience a different effective magnetic field.[17]

In preliminary work,[18] we showed that modeling the additional off-resonance experienced by myelin water reduces the Cramér-Rao Lower Bound (CRLB) of estimates of MWF using small-tip fast recovery (STFR) MRI.[19] We showed that the STFR sequence is sensitive to the frequency differences, suggesting that the difference in off-resonance between myelin and non-myelin water is a potentially useful contrast mechanism containing information that can help estimate MWF.[18] Simulations using optimized STFR scan parameters led to MWF estimates with lower errors when there was a fixed, nonzero (but unknown) difference in off-resonance, compared to when there was no (still unknown) frequency difference. To our knowledge, this work was the first to specifically design scans for myelin water imaging that exploit frequency differences. Because the actual frequency difference is unknown and might vary between voxels or disease conditions, the proposed approach treats the difference as an unknown parameter that is estimated alongside other unknown parameters like the T_1 and T_2 values of the various tissue compartments.

One limitation of our previous work was its tissue model. In[18] we assumed a 2-compartment, non-exchanging model for simplicity in computing the STFR signal. However, neglecting exchange can lead to biases in MWF estimates.[20] Therefore, the method proposed in this paper uses a 3-compartment model. The 3 compartments are myelin water, non-myelin water, and a macromolecular pool; myelin water and non-myelin water are in exchange, while myelin water exchanges with the macromolecular pool.[21]

We previously estimated MWF from optimized STFR scans using parameter estimation via regression with kernels (PERK), a recently developed learning-based technique for parameter estimation in MRI that uses kernel ridge regression at its core.[18,22] One alternative method for MWF estimation is non-linear least squares, which requires iterative methods for solving and can get stuck in a local minimum. Another alternative is dictionary search, which requires evaluating the STFR signal model on a discretized grid of the signal model parameters, which is impractical when the number of parameters exceeds 3 or 4. Yet another alternative is to use a neural network. While neural networks can lead to good parameter estimates, they require a lot of training data and long training time. In contrast, PERK trains quickly and avoids the other problems associated with non-linear least squares and dictionary search. Therefore, this work again uses PERK.

This paper substantially builds upon our previous work. First, we re-optimize the STFR scan parameters to model variations of bulk off-resonance and to account for 2 spoiled gradient-recalled echo (SPGR) scans that are used for separate bulk off-resonance estimation. Next, we compare STFR-based MWF estimates to MESE-based MWF estimates in simulation. In particular, we estimate MWF from the optimized STFR scans with PERK[22] using a 3-compartment tissue model with exchange. Finally, we compare our proposed STFR-based MWF estimation method to MESE-based MWF estimation in vivo. Figure 1 illustrates the proposed approach.

The organization of this paper is as follows. Section 1.1 provides background information on the scans used in this work (STFR and MESE), the scan design process, and PERK. Section 2 outlines our experiments, both for the STFR scan design and for MWF estimation in simulation and in vivo. Section 3 reports the experimental results. Section 4 discusses our results. Section 5 gives concluding remarks.

1.1 | Background

1.1.1 | STFR

One repetition of STFR[19] begins with an initial tip-down excitation with flip angle α. Then there is time T_{free} during which free precession occurs, after which there is a tip-up excitation ("fast recovery") where magnetization is rotated up toward the +z-axis with flip angle β and phase ϕ. Finally, there is gradient spoiling for time T_g. For a single compartment, the signal obtained at a given spatial location from a STFR scan is given by[23]

$$s_1(M_0, T_1, T_2, \Delta\omega, \kappa, T_{\text{free}}, T_g, \alpha, \beta, \phi) = \frac{M_0 \sin(\kappa\alpha)\left[e^{-T_g/T_1}\left(1-e^{-T_{\text{free}}/T_1}\right)\cos(\kappa\beta)+\left(1-e^{-T_g/T_1}\right)\right]e^{-T_{\text{free}}/(2T_2)}e^{-i\Delta\omega T_{\text{free}}/2}}{1-e^{-T_g/T_1}e^{-T_{\text{free}}/T_2}\sin(\kappa\alpha)\sin(\kappa\beta)\cos(\Delta\omega\cdot T_{\text{free}}-\phi)-e^{-T_g/T_1}e^{-T_{\text{free}}/T_1}\cos(\kappa\alpha)\cos(\kappa\beta)}, \quad (1)$$

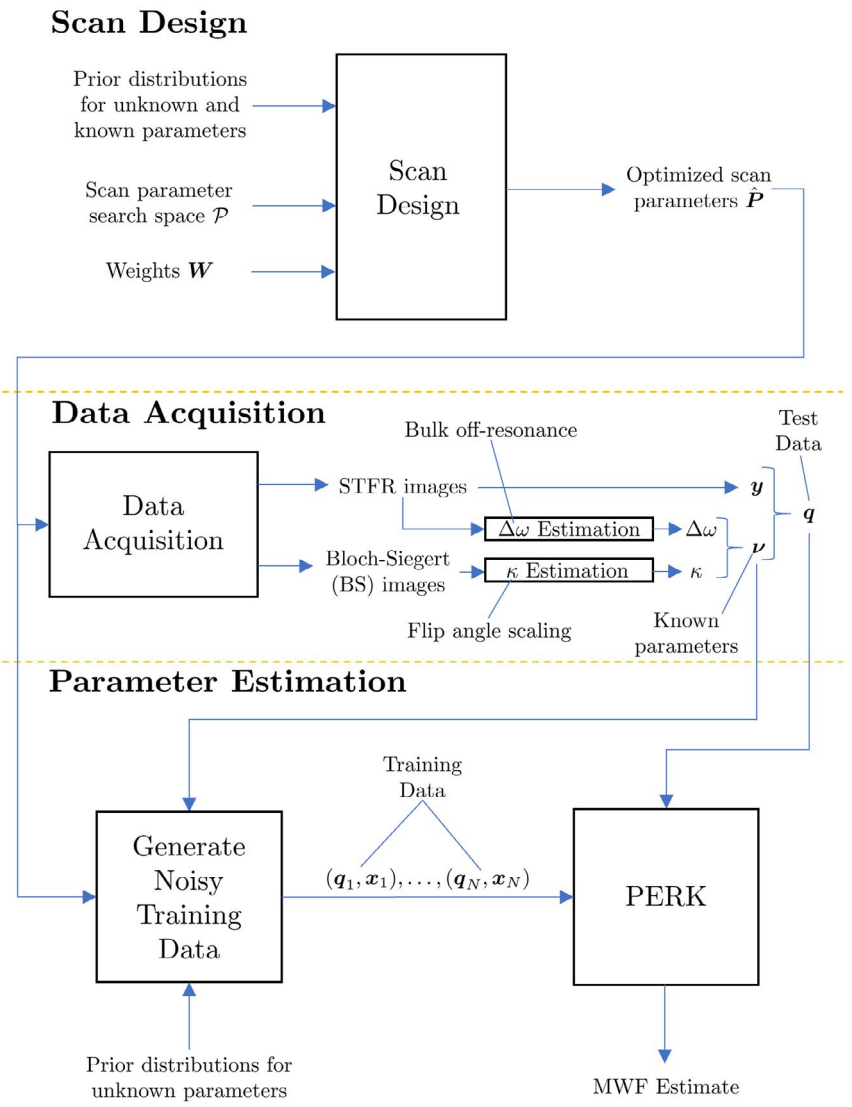

FIGURE 1 Workflow of the proposed methods. We first optimized a set of STFR scan parameters by minimizing a Cramér-Rao Lower Bound, then acquired data using those scans, as well as Bloch-Siegert (BS) scans. Two of the STFR scans were equivalent to SPGR scans, so were used to estimate $\Delta\omega$, and the BS scans were used to estimate κ. These parameters were treated as known values in the MWF estimation step. We then generated noisy training data using an STFR signal model. Finally, we passed the training data, acquired STFR images, and known parameters to PERK to estimate MWF voxel-by-voxel

where M_0 is the equilibrium magnetization, T_1 and T_2 are the spin-lattice and spin-spin time constants, respectively, $\Delta\omega$ is the off-resonance frequency, and κ is a flip angle scaling constant (to account for differences between the prescribed and actual flip angles). Note that approximating flip angle error as a scale factor is accurate for the small flip angles used in this work, but typically inaccurate at larger flip angles. STFR with $\beta = 0$ is the same as SPGR with $T_R = T_{free} + T_g$.

For myelin water imaging, more than 1 compartment must be modeled. In a 2-compartment model, 1 compartment consists of spins within myelin (myelin water), and the other compartment consists of other spins (non-myelin water). If one neglects exchange, then the STFR signal at a given spatial location is the weighted sum of the single-compartment STFR signals of the individual compartments:

$$\begin{aligned} s_2(M_0, f_f, T_{1,f}, T_{1,s}, T_{2,f}, T_{2,s}, \Delta\omega_f, \Delta\omega, \kappa, T_{free}, T_g, \alpha, \beta, \phi) \\ = f_f \cdot s_1(M_0, T_{1,f}, T_{2,f}, \Delta\omega + \Delta\omega_f, \kappa, T_{free}, T_g, \alpha, \beta, \phi) \\ + (1 - f_f) \cdot s_1(M_0, T_{1,s}, T_{2,s}, \Delta\omega, \kappa, T_{free}, T_g, \alpha, \beta, \phi), \end{aligned} \quad (2)$$

where the weight f_f is the MWF, $T_{1,f}$ and $T_{2,f}$ are the T_1 and T_2 time constants for the fast-relaxing, myelin water compartment, $T_{1,s}$ and $T_{2,s}$ are the T_1 and T_2 time constants for the slow-relaxing, non-myelin water compartment, and $\Delta\omega_f$ is the additional off-resonance that is experienced only by myelin water.[17]

Although (2) has a convenient analytical expression, a more accurate tissue model for cerebral WM consists of 3 compartments (non-myelin water, myelin water, and a macromolecule water pool) with exchange between the non-myelin and myelin water compartments and from the myelin water compartment to the macromolecule compartment.[21] In this case, the STFR signal is also a function of the macromolecule compartment volume fraction f_m, the macromolecule compartment $T_{1,m}$ and $T_{2,m}$, the residence time for exchange from myelin water to non-myelin water $\tau_{f \to s}$, and the residence time for exchange from myelin water to the macromolecule compartment $\tau_{f \to m}$, in addition to the previously mentioned parameters. We assume the myelin water and non-myelin water compartments are in chemical equilibrium, which means that $f_f \tau_{s \to f} = (1 - f_f - f_m)\tau_{f \to s}$,

and we assume there is no other exchange, that is, $\tau_{m\to f} = \tau_{s\to m} = \tau_{m\to s} = \infty$.[21] Because of exchange, the STFR signal no longer has an analytical expression and must be computed using the Bloch-McConnell equation.[24]

1.1.2 | MESE

One repetition of MESE[25] consists of an initial excitation with flip angle α_{ex} (typically 90°) followed by a sequence of N_{ref} refocusing excitations with flip angle α_{ref} (typically 180°). The signal is sampled at times $T_E, 2T_E, \ldots, N_{ref}T_E$ after the initial excitation, resulting in N_{ref} images in 1 MESE scan. The repetition time T_R is typically chosen to be long enough so that the net magnetization of the spins is in equilibrium prior to each repetition. Thus, the MESE signal is a function of α_{ex}, α_{ref}, T_E, and T_R, as well as the same tissue parameters as the STFR signal; but if T_R is sufficiently long there is little dependence on T_1 (of any compartment). Additionally, for myelin water imaging using MESE, normally the acquired MESE signal is modeled as a weighted sum of MESE signals from individual compartments, ignoring exchange between compartments. When ignoring exchange, we computed the MESE signal using the extended phase graph (EPG) method.[26] When accounting for exchange, we used Bloch-McConnell simulation.

1.1.3 | Scan design using the CRLB

MR image data for a single voxel in a single scan are often modeled as

$$y = f(\boldsymbol{x}, \boldsymbol{\nu}, \boldsymbol{p}) + \epsilon, \tag{3}$$

where $f(\boldsymbol{x}, \boldsymbol{\nu}, \boldsymbol{p}) \in \mathbb{C}$ is the MR signal that is a function of unknown parameters $\boldsymbol{x}$, known parameters $\boldsymbol{\nu}$, and scan parameters $\boldsymbol{p}$; and $\epsilon \sim \mathbb{C}\mathcal{N}(0, \sigma^2)$ is additive complex Gaussian noise. When there are D scans then the data for a single voxel across each scan is collected into a vector:

$$\boldsymbol{y} = \boldsymbol{f}(\boldsymbol{x}, \boldsymbol{\nu}, \boldsymbol{P}) + \boldsymbol{\epsilon}, \tag{4}$$

where $\boldsymbol{y} \in \mathbb{C}^D$, $\boldsymbol{f}(\boldsymbol{x}, \boldsymbol{\nu}, \boldsymbol{P}) = [f_1(\boldsymbol{x}, \boldsymbol{\nu}, \boldsymbol{p}_1), \ldots, f_D(\boldsymbol{x}, \boldsymbol{\nu}, \boldsymbol{p}_D)]^T$, f_d is the signal given by the dth scan for $d = 1, \ldots, D$, $\boldsymbol{P} = (\boldsymbol{p}_1, \ldots, \boldsymbol{p}_D)$ denotes the collection of all scan parameters, and the noise vector is $\boldsymbol{\epsilon} \sim \mathbb{C}\mathcal{N}(\boldsymbol{0}, \boldsymbol{\Sigma})$. We assume that each scan has noise independent of the other scans, and we assume that each scan has the same noise variance σ^2; thus $\boldsymbol{\Sigma} = \sigma^2 \boldsymbol{I}_D$, where $\boldsymbol{I}_D$ is the $D \times D$ identity matrix.

For simplicity in computing the Fisher information matrix (see below), we further assume that the MR signal model f is real-valued. We also take the magnitude of the received signal y, resulting in a Rician distributed signal[27]; however, we assume sufficiently high SNR so that this magnitude signal is approximately normally distributed with mean $f(\boldsymbol{x}, \boldsymbol{\nu}, \boldsymbol{p})$ and variance σ^2.

Under these assumptions, the Fisher information matrix for the magnitude of signal model (4) is[28]

$$\boldsymbol{I}(\boldsymbol{x}, \boldsymbol{\nu}, \boldsymbol{P}) = \frac{1}{\sigma^2}(\nabla_{\boldsymbol{x}} \boldsymbol{f}(\boldsymbol{x}, \boldsymbol{\nu}, \boldsymbol{P}))^T (\nabla_{\boldsymbol{x}} \boldsymbol{f}(\boldsymbol{x}, \boldsymbol{\nu}, \boldsymbol{P})), \tag{5}$$

where $\nabla_{\boldsymbol{x}}$ denotes a row gradient with respect to the unknown parameters $\boldsymbol{x}$. The inverse Fisher information matrix gives the CRLB for unbiased estimators.[29] In particular, the variance of an unbiased estimator for the ith unknown parameter x_i has a lower bound given by the ith diagonal element of the inverse Fisher information matrix, that is, $\mathrm{var}(\hat{x}_i) \geq [(\boldsymbol{I}(\boldsymbol{x}, \boldsymbol{\nu}, \boldsymbol{P}))^{-1}]_{i,i}$. This bound on the precision of unbiased estimators is useful for optimizing experimental designs. The CRLB has been used to optimize MR sequence parameters for a variety of pulse sequences and applications (eg, Refs. 22,30-32). In this work, we optimize scan parameters of a set of D STFR scans for MWF estimation by minimizing an expected weighted sum of the CRLB for each unknown parameter[33]:

$$\hat{\boldsymbol{P}} = \mathrm{argmin}_{\boldsymbol{P} \in \mathcal{P}} \mathbb{E}_{\boldsymbol{x}, \boldsymbol{\nu}} [\mathrm{trace}(\boldsymbol{W}(\boldsymbol{I}(\boldsymbol{x}, \boldsymbol{\nu}, \boldsymbol{P}))^{-1})], \tag{6}$$

where $\mathcal{P}$ denotes the scan parameter search space, $\mathbb{E}_{\boldsymbol{x},\boldsymbol{\nu}}$ denotes an expectation over $\boldsymbol{x}$ and $\boldsymbol{\nu}$, and $\boldsymbol{W}$ is a diagonal weighting matrix used to indicate the relative importance of precisely estimating the different unknown parameters.

1.1.4 | Parameter estimation via regression with kernels (PERK)

This section describes the PERK method we use to estimate the MWF from STFR scans. Suppose a set of scan parameters $\boldsymbol{P}$ is given, typically the $\hat{\boldsymbol{P}}$ from the scan design process (6). We seek to estimate unknown parameters $\boldsymbol{x}$ after acquiring data using the D scans corresponding to these scan parameters. We generate training data by simulating data $\boldsymbol{y}_n$ via (4) with appropriate signal models $\boldsymbol{f}$ for various values of unknown and known parameters $\boldsymbol{x}_n$ and $\boldsymbol{\nu}_n$; these N training data points are collected as $(\boldsymbol{q}_1, \boldsymbol{x}_1), \ldots, (\boldsymbol{q}_N, \boldsymbol{x}_N)$, where $\boldsymbol{q}_n = [|\boldsymbol{y}_n|^T, \boldsymbol{\nu}_n^T]^T$ and $|\cdot|$ denotes element-wise complex modulus. After scanning (with the scan parameters $\boldsymbol{P}$), we have test data $\boldsymbol{q}$ for each voxel (where $\boldsymbol{\nu}$ collects separately estimated parameters, such as B_1^+ maps, that are treated as known values), and we want to estimate $\boldsymbol{x}$. PERK computes estimates via regularized linear regression (ridge regression), after first transforming the feature vectors $\boldsymbol{q}$ (for both training and testing) via some user-defined feature map (which

is never directly used but is indirectly specified through the choice of kernel function). The PERK estimator is[22]

$$\hat{\boldsymbol{x}}(\boldsymbol{q}) = \frac{1}{N}\boldsymbol{X}\boldsymbol{1}_N + \boldsymbol{X}\boldsymbol{M}(\boldsymbol{M}\boldsymbol{K}\boldsymbol{M} + N\rho\boldsymbol{I}_N)^{-1}\boldsymbol{k}(\boldsymbol{q}), \tag{7}$$

where $\boldsymbol{X} = [\boldsymbol{x}_1, \ldots, \boldsymbol{x}_N]$ denotes all of the training data, $\boldsymbol{1}_N \in \mathbb{R}^N$ is a vector of all ones, $\boldsymbol{M} = \boldsymbol{I}_N - \frac{1}{N}\boldsymbol{1}_N\boldsymbol{1}_N^T$ is a de-meaning operator, ρ is a regularization parameter, the Gram matrix $\boldsymbol{K} \in \mathbb{R}^{N\times N}$ has entries $K_{i,j} = k(\boldsymbol{q}_i, \boldsymbol{q}_j)$, and $\boldsymbol{k}(\boldsymbol{q}) = [k(\boldsymbol{q}, \boldsymbol{q}_1), \ldots, k(\boldsymbol{q}, \boldsymbol{q}_N)]^T - \frac{1}{N}\boldsymbol{K}\boldsymbol{1}_N$, where $k(\boldsymbol{q}, \boldsymbol{q}')$ is the user-specified kernel function. In this work, we used the Gaussian kernel

$$k(\boldsymbol{q}, \boldsymbol{q}') \triangleq \exp\left(-\frac{1}{2}\|\boldsymbol{\Lambda}^{-1}(\boldsymbol{q} - \boldsymbol{q}')\|_2^2\right), \tag{8}$$

where $\boldsymbol{\Lambda}$ is a positive definite weighting matrix. PERK with a Gaussian kernel corresponds to first transforming the feature vectors $\boldsymbol{q}$ via a nonlinear feature map into infinite-dimensional features, and then applying ridge regression on the transformed features. This lifting of features to a higher dimensional space improves the ability to capture the nonlinear dependence of the signal on the unknown parameters we wish to estimate.

To reduce storage and computational needs, we approximated (7) using random Fourier features.[22,34]

2 | METHODS

This section describes the experiments performed in this work. We first explain the scan design process for optimizing a set of STFR scans for MWF estimation. We then explain simulated MWF estimation experiments that compare our proposed method to MESE-based MWF estimation. Finally, we explain an experiment to test our proposed method in vivo. The code for reproducing the methods and results in this paper is available at https://github.com/StevenWhitaker/STFR-MWF. The raw data are available at https://doi.org/10.7302/nw6e-1d66.

2.1 | Scan design

For the STFR scan design, we computed the CRLB using the 2-compartment non-exchanging signal model (2). We chose the weighting matrix $\boldsymbol{W}$ to place full weight on the CRLB for f_f (ie, the diagonal entries of $\boldsymbol{W}$ were all 0 except for a 1 in the location corresponding to f_f). We took the flip angle scaling κ and bulk off-resonance $\Delta\omega$ to be known, that is, part of $\boldsymbol{\nu}$, and we optimized a set of $D = 11$ STFR scans. Two of these scans were SPGR scans with fixed scan parameters and an echo time shift. We included these scans to enable the option of estimating $\Delta\omega$ using conventional techniques and then treat $\Delta\omega$ as known for further parameter estimation.

We fixed $T_g = 2.8$ ms across all 11 scans. We fixed $\alpha = 5°$ and $T_{free} = 10.3$ ms for the 2 SPGR scans. The T_E of each STFR scan and the first SPGR scan was 4 ms. The echo time shift between the 2 SPGR scans was 2.3 ms. For the remaining 9 STFR scans, we fixed $T_{free} = 8$ ms and we constrained $\alpha \in [1, 15]°$, $\beta \in [0, 15]°$, and $\phi \in [-180, 180]°$.

The expectation in (6) requires choices for the probability distributions of the unknown and known parameters. Table 1 shows the distributions we used. To explore the effect that the additional myelin water off-resonance $\Delta\omega_f$ has on the CRLB of f_f, we performed 1 scan design (design A) where we took $\Delta\omega_f$ to be unknown, and another (design B) where we ignored $\Delta\omega_f$ (ie, we assumed it was known and equal to 0). To solve the optimization in (6), we used the NLopt package (https://github.com/JuliaOpt/NLopt.jl) in the Julia programming language (https://julialang.org).

2.2 | MWF estimation

For MWF estimation, we compared several estimation protocols. The proposed method, which we call STFR3-PERK, uses PERK to estimate MWF from the optimized STFR scans, with training data generated using the 3-compartment exchanging model. This method assumes bulk off-resonance $\Delta\omega$ and flip angle scaling κ are known (unless otherwise noted). Another method, STFR2-PERK, is the same as STFR3-PERK, except training data are generated using the 2-compartment non-exchanging model. Again, $\Delta\omega$ and κ are assumed known. The reference method, MESE-NNLS, uses regularized NNLS to estimate MWF from a MESE scan. Following,[5] we fit 40 different T_2 components spaced logarithmically from 15 ms to 2000 ms, and computed MWF as the proportion of signal coming from components with $T_2 \leq 40$ ms to the total signal. This method does not assume knowledge of $\Delta\omega$ or κ, but jointly estimates κ. A fourth method, MESE-PERK, estimates MWF from a MESE scan using PERK, with training data generated using the 3-compartment exchanging model. This method was included to determine whether performance differences were due to the estimation method (ie, NNLS versus PERK), or due to the scans (ie, MESE versus STFR). MESE-PERK does not assume knowledge of $\Delta\omega$ or κ. Finally, because the proposed STFR3-PERK assumes $\Delta\omega$ and κ are known, whereas the reference MESE-NNLS does not, we compared a fifth method, STFR3-PERK-JE, that is the same as STFR3-PERK except $\Delta\omega$ and κ are assumed unknown. Table 1 shows the training ranges for the methods that use PERK.

The methods that use PERK require specifying the regularization parameter ρ and the positive definite matrix $\boldsymbol{\Lambda}$ in the Gaussian kernel. For the Gaussian kernel, to eliminate

TABLE 1 Unknown and known parameters used in scan design and in simulation

Parameter	Design A	Design B	White matter	Gray matter	PERK training ranges
M_0	1	1	0.77	0.86	$\text{unif}(0, M_0^{\max})$[a]
f_f	unif (0.03, 0.31)	unif (0.03, 0.31)	0.15	0.03	unif (0.03, 0.31)
$T_{1,f}$ (ms)	$\mathcal{N}(400, 80^2)$	$\mathcal{N}(400, 80^2)$	400	500	unif (320,480)
$T_{1,s}$ (ms)	$\mathcal{N}(1000, 200^2)$	$\mathcal{N}(1000, 200^2)$	832	1331	unif (800, 1200)
$T_{2,f}$ (ms)	$\mathcal{N}(20, 4^2)$	$\mathcal{N}(20, 4^2)$	20	20	unif (16, 24)
$T_{2,s}$ (ms)	$\mathcal{N}(80, 16^2)$	$\mathcal{N}(80, 16^2)$	80	80	unif (64, 96)
$\Delta\omega_f$ (Hz)	unif (5, 35)	0[c]	15	5	unif (0, 35)
$\Delta\omega$ (Hz)	unif (−50, 50)[c]	unif (−50, 50)[c]	Varies	Varies	$\text{unif}(-50, 50)$[b]
κ	unif (0.8, 1.2)[c]	unif (0.8, 1.2)[c]	Varies	Varies	$\text{unif}(0.8, 1.2)$[b]
f_m	N/A	N/A	0.1	0.03	unif (0.03, 0.31)
$T_{1,m}$ (ms)	N/A	N/A	1000	1000	unif (800, 3000)
$T_{2,m}$ (ms)	N/A	N/A	0.02	0.02	unif (0.01, 0.1)
$\tau_{f\to s}$ (ms)	N/A	N/A	100	20	unif (80, 150)
$\tau_{f\to m}$ (ms)	N/A	N/A	50	10	unif (40, 75)

Notes: Values were chosen to match literature values for white matter.[1,17,21,35] We used $M_0 = 1$ for the scan designs because it only scales the STFR signal. The line below κ separates parameters used in both the 2-compartment and 3-compartment models (above) from those used only in the 3-compartment exchanging model (below).

N/A—Not applicable (scan designs only used 2-compartment model).

unif (a, b)—Uniform distribution on interval $[a, b]$.

$\mathcal{N}(\mu, \sigma^2)$—Normal distribution with mean μ and variance σ^2.

[a]$M_0^{\max}$ given by maximum signal value from data divided by mean signal value from signal model with $M_0 = 1$.

[b]Unless parameter is known, in which case training range covers range of values in known map.

[c]Known parameter.

dependence on scale we set $\mathbf{\Lambda} = \lambda \text{diag}(\boldsymbol{m}_{|\boldsymbol{q}|})$, where λ is a regularization parameter and $\boldsymbol{m}_{|\boldsymbol{q}|}$ denotes the sample average across all voxels of the magnitude test data $|\boldsymbol{q}|$, where $\boldsymbol{q}$ collects the magnitude STFR signals $|\boldsymbol{y}|$ and the known parameters $\boldsymbol{\nu}$ (see § 1.1.4). We chose $\rho = 2^{-60}$ and $\lambda = 2^{3.5}$ for the regularization parameters, which we tuned using a holdout process described in [[22], Section S.II].

2.2.1 | Numerical simulation

We compared the 2 optimized sets of STFR scans to validate the scan design process. We simulated test data using the 2-compartment non-exchanging STFR signal model (2) using the range of tissue parameters over which the scans were optimized (to match the scan design assumptions), and we estimated MWF using STFR2-PERK. We measured the root mean square error (RMSE) of the MWF estimates versus the additional myelin water off-resonance $\Delta\omega_f$ for 3 cases: first, using design B and training data that ignored $\Delta\omega_f$ (ie, all training points had $\Delta\omega_f = 0$); second, using design B and training data that accounted for $\Delta\omega_f$; and third, using design A and training data that accounted for $\Delta\omega_f$. Section S1 of the Supporting Information describes another experiment where test data was generated using the 2-compartment model with fixed WM and gray matter (GM) tissue values (see Table 1).

Next, we investigated the effects of exchange and compared STFR-based MWF estimates to MESE-based estimates. We simulated STFR scans using design A and a MESE scan using $\alpha_{ex} = 90°$, $\alpha_{ref} = 180°$, $N_{ref} = 32$, $T_E = 10$ ms, and $T_R = 1200$ ms. We simulated test data using the 3-compartment model with exchange and tissue parameters corresponding to WM and GM (see Table 1). Additionally, we chose bulk off-resonance $\Delta\omega$ values to vary from −30 to 30 Hz and κ values to vary from 0.8 to 1.2. We compared MWF estimates from each of the aforementioned methods (STFR3-PERK, STFR2-PERK, MESE-NNLS, MESE-PERK, and STFR3-PERK-JE). For these simulations we added complex Gaussian noise corresponding to a SNR in WM ranging from 7 to 28 across the STFR scans and from 2 to 122 across the 32 MESE echoes (to match the SNR of the in vivo data), where SNR was calculated by dividing the WM signal mean by the noise SD.

The proposed method (STFR3-PERK) uses a model that matches the model used to generate the test data in the previous experiment. To investigate the effects of model mismatch, we repeated the previous experiment using a 9-compartment

tissue model with exchange for the test data. The 9 compartments were created by splitting each of the 3 compartments in the 3-compartment model into 3 sub-compartments. For example, the myelin water compartment with fraction f_f and relaxation time $T_{2,f}$ was split into 3 compartments with fractions $0.5f_f$, $0.25f_f$, and $0.25f_f$ and relaxation times $T_{2,f}$, $0.8T_{2,f}$, and $1.2T_{2,f}$. Section S2 of the Supporting Information repeats this experiment for a 4-compartment model with exchange and a 3-compartment model without exchange.

2.2.2 | In vivo experiments

Under an IRB-approved protocol, we scanned a healthy volunteer to compare the proposed STFR-based MWF estimation to MESE-based MWF estimation. We used 3D acquisitions for both the STFR and MESE scans to avoid slice profile effects. The STFR scans used design A, and the RF pulses had time-bandwidth product of 8 and duration of 1 ms; the 2 SPGR scans took 58 seconds and the 9 STFR scans took 3 minutes 36 seconds for a total scan time of 4 minutes 34 seconds. We also acquired a pair of Bloch-Siegert (BS) scans for separate estimation of κ[36]; the excitation RF pulse of these scans had time-bandwidth product of 8 and duration of 1 ms, and used $\pm$4 kHz off-resonant Fermi pulses between excitation and readout. The total duration of the BS scans was 2 minutes 40 seconds. Therefore, our overall STFR-based MWF estimation scan protocol lasted 7 minutes 14 seconds. For the MESE scan, we used the same scan parameters as in simulation (described above); the initial excitation RF pulse had time-bandwidth product of 6, duration of 3 ms, and slab thickness of 0.9 cm, and each refocusing pulse had time-bandwidth product of 2, duration of 2 ms, and slab thickness of 2.1 cm. Each refocusing pulse was also flanked with crusher gradients, each of which imparted 14 cycles of phase across the imaging volume. The total duration of the MESE scan was 36 minutes 11 seconds. For all scans, we acquired a $22 \times 22 \times 0.99\,\text{cm}^3$ field of view (FOV) with matrix size $200 \times 200 \times 9$ (except the BS scans used matrix size $200 \times 50 \times 9$). We implemented the protocol in TOPPE.[37]

We used a GE Discovery™ MR750 3.0T scanner with a 32-channel Nova Medical® head coil. We used conventional inverse FFT reconstruction followed by square-root of sum-of-squares coil combination to make the magnitude images used for MWF estimation. We estimated the SNR in the WM brain regions (pooling the 4 WM regions of interest (ROIs) in Supporting Information Figure S1 for each scan/echo) to vary from 8 to 17 across the STFR scans and from 6 to 73 for across MESE echoes.

We analyzed the center slice of the acquired data. We estimated MWF using STFR3-PERK, STFR2-PERK, MESE-NNLS, and MESE-PERK. In this case, for STFR3-PERK and STFR2-PERK we took bulk off-resonance $\Delta\omega$ to be unknown (but still assumed κ to be known).

3 | RESULTS

3.1 | Scan design

Table 2 reports the 2 optimized scan design parameters. For design A, the additional myelin water off-resonance $\Delta\omega_f$ was taken to be unknown and distributed uniformly from 5 to 35 Hz. For design B, $\Delta\omega_f$ was ignored (ie, taken to be known and equal to 0).

Figure 2 compares the expected CRLB of the SD of MWF of these 2 scan designs versus $\Delta\omega_f$, where at each data point $\Delta\omega_f$ is fixed (unlike the other parameters that vary according to the distributions in Table 1) but is still unknown, that is, contained in $\boldsymbol{x}$ (see §1.1.3). For these CRLB calculations, we used a noise SD that corresponds to SNR ranging from 9 to 15 in WM across the STFR scans to match the SNR of the 1.1 mm isotropic in vivo data. Figure 2 shows that modeling $\Delta\omega_f$ improves the precision of the optimized scan design, and that MWF becomes easier to estimate as $\Delta\omega_f$ increases.

TABLE 2 Optimized scan parameters

	Scan #	1	2	3	4	5	6	7	8	9	10	11
Design A	α	5	5	15.0	15.0	15.0	15.0	15.0	15.0	15.0	11.4	15.0
	β	0	0	15.0	15.0	11.6	15.0	13.3	15.0	14.9	0.3	14.4
	ϕ	0	0	−139.3	−108.1	−66.0	−28.0	25.9	64.4	104.1	146.3	173.0
Design B	α	5	5	15.0	15.0	15.0	15.0	15.0	15.0	15.0	15.0	15.0
	β	0	0	15.0	14.5	14.9	14.8	14.8	14.9	0.0	14.5	15.0
	ϕ	0	0	−139.3	−113.3	−63.7	−14.3	14.3	63.7	83.2	113.3	139.3

Notes: The first 2 scans are the STFR (SPGR) scans with fixed parameters; the remaining scans were optimized during the scan design process. All values have units of degrees. For design A, the additional myelin water off-resonance $\Delta\omega_f$ was taken to be unknown and distributed uniformly from 5 to 35 Hz. For design B, $\Delta\omega_f$ was ignored (ie, taken to be known and equal to 0).

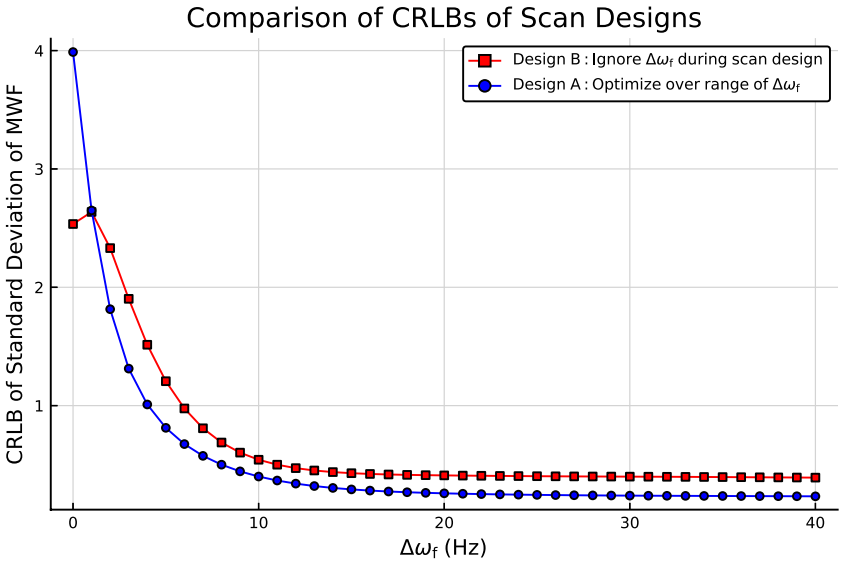

FIGURE 2 The 2 optimized scans (see Table 2) were evaluated to explore how including the additional myelin water off-resonance $\Delta\omega_f$ in the design process affects performance. Design A (where $\Delta\omega_f$ was included in the optimization) has a better expected CRLB for every value of $\Delta\omega_f$ within the 5-35 Hz range over which design A was optimized. Design B (where $\Delta\omega_f$ was ignored) understandably has a better expected CRLB for $\Delta\omega_f = 0$. For each value of $\Delta\omega_f$ investigated in this plot, the expected CRLB was computed with that value of $\Delta\omega_f$ held constant but unknown. Typical values of $\Delta\omega_f$ in white matter are 5-35 Hz.[17] Although these CRLB values predict estimator SD (for an unbiased estimator) on the order of 100% MWF or more, we are not restricted by these large values because we are using a Bayesian estimator (see Supporting Information Figure S6 for details)

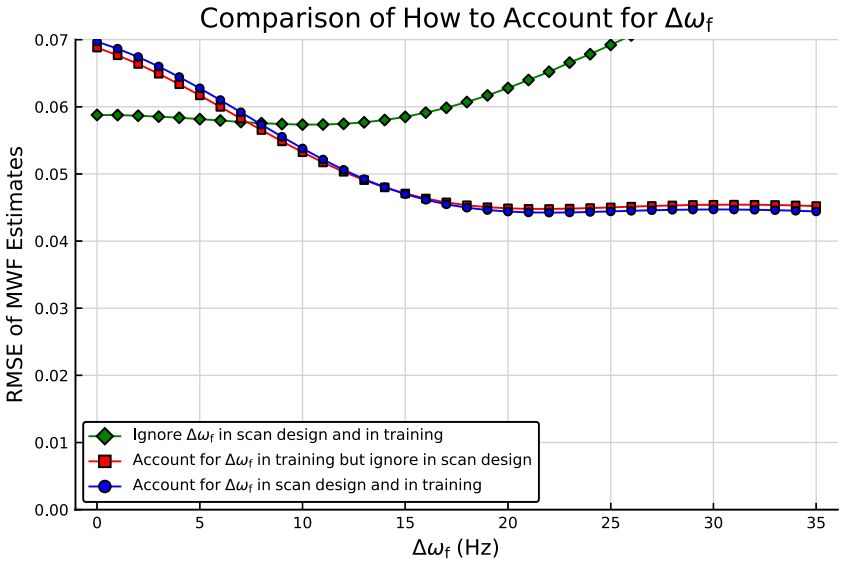

FIGURE 3 RMSE of MWF estimates from simulated test data for various ways of accounting for the additional myelin water off-resonance $\Delta\omega_f$. The diamond-markered green curve was generated using scan design B (where $\Delta\omega_f$ was ignored) and using PERK training data where $\Delta\omega_f = 0$. In other words, $\Delta\omega_f$ was not considered in any aspect, neither in the scan design nor when training. The square-markered red curve was also generated using scan design B, but the training data included a range of $\Delta\omega_f$ values. The circle-markered blue curve was generated using design A and a range of values of $\Delta\omega_f$. The latter 2 methods look almost identical, but both have much better RMSE than the first method as $\Delta\omega_f$ increases

3.2 | MWF estimation

3.2.1 | Numerical simulation

We computed the RMSE of MWF estimates for test data generated using (2) with different values of $\Delta\omega_f$ and a range of tissue parameters. For design A, we estimated MWF using training data that were generated with a range of $\Delta\omega_f$ values. For design B, in 1 experiment we estimated MWF using training data that was generated with a range of $\Delta\omega_f$, and in another experiment the training data included only $\Delta\omega_f = 0$. Figure 3 shows the results. The mean MWF value in the

test data was 0.17, so the minimum RMSE of 0.045 corresponds to about 26% relative error. Supporting Information Figure S2 reports an analogous experiment using fixed WM and GM tissue values.

Furthermore, we investigated the effects of exchange on MWF estimates. We simulated STFR scans (using design A) and a MESE scan, and we used the 3-compartment tissue model with exchange using tissue parameters corresponding to WM and GM. We estimated MWF using STFR2-PERK, STFR3-PERK, MESE-NNLS, MESE-PERK, and STFR3-PERK-JE. Table 3 shows the RMSEs, means, and SDs of the MWF estimates. Figure 4 shows the ground truth map and a visual comparison of the estimated MWF maps. Figure 5 shows the results of this experiment when using a 9-compartment exchanging model. Supporting Information Figures S3 and S4 show results when using a 4-compartment exchanging model and a 3-compartment non-exchanging model, respectively. The anatomy for the simulated data used in these experiments came from BrainWeb.[38]

3.2.2 | In vivo experiments

We scanned a healthy volunteer using scan design A. Supporting Information Figure S5 shows images of the 2 SPGR and 9 STFR scans of the subject. In the same scan session, we also scanned the volunteer with a MESE scan. Figure 6 shows MWF maps that were computed from the STFR and MESE scans. In this case, we made the STFR-based MWF estimates without using a separately estimated $\Delta\omega$ map because the MWF estimates made with the separately estimated $\Delta\omega$ map exhibited spatial variation that mimicked the field map spatial variations, which we do not expect in MWF maps (ie, we expect myelin content to be independent of $\Delta\omega$). Table 4 shows numerical results for the in vivo data for several ROIs.

4 | DISCUSSION

Almost all of the optimized flip angles α and β for both scan designs A and B are equal to (or are very close to) the upper

TABLE 3 Comparison of various methods of MWF estimation

	White matter (MWF = 0.15)			Gray matter (MWF = 0.03)			
	RMSE	**Mean**	**SD**	**RMSE**	**Mean**	**SD**	**Time (s)**
STFR2-PERK	0.215	0.349	0.082	0.185	0.209	0.047	**21.9**
STFR3-PERK	**0.021**	0.158	**0.020**	0.046	0.074	0.015	43.1
STFR3-PERK-JE	0.026	**0.145**	0.026	0.044	0.069	0.021	41.3
MESE-NNLS	0.063	0.092	0.025	0.029	0.001	**0.003**	1602.4
MESE-PERK	0.029	0.134	0.025	**0.026**	**0.026**	0.025	142.7

Notes: The reported time refers to the entire estimation, combining the time to estimate MWF in white matter voxels and gray matter voxels; it also includes training time for the methods that use PERK. The best value in each column is highlighted. See Figure 4 for a visual comparison of these methods.

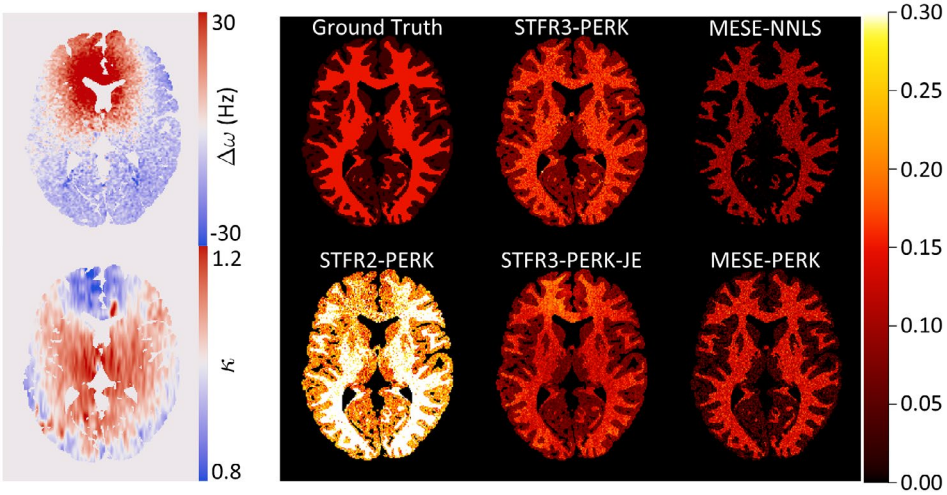

FIGURE 4 Right: MWF maps from 5 methods using simulated test data for a 3-compartment tissue model with exchange. Table 3 reports numerical results. The proposed STFR3-PERK estimates are closer to the true MWF value for white matter tissue values than are the MESE-NNLS estimates. Left: Bulk off-resonance $\Delta\omega$ and flip angle scaling κ maps used in this simulation

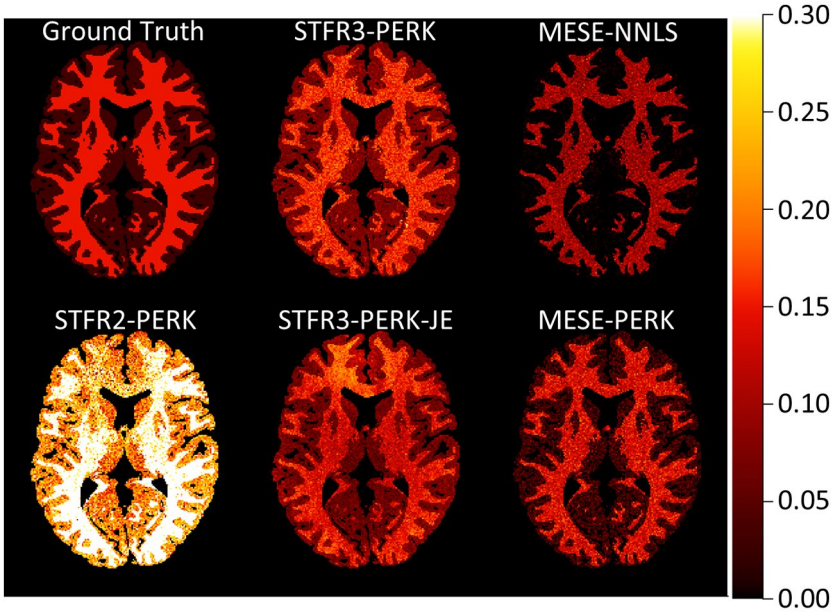

FIGURE 5 MWF maps from 5 methods using simulated test data for a 9-compartment tissue model with exchange. These results are essentially the same as when using the 3-compartment exchanging model (see Figure 4). Thus, even though STFR3-PERK was trained with a 3-compartment exchanging model, it still produced good MWF estimates from signal generated using a 9-compartment exchanging model

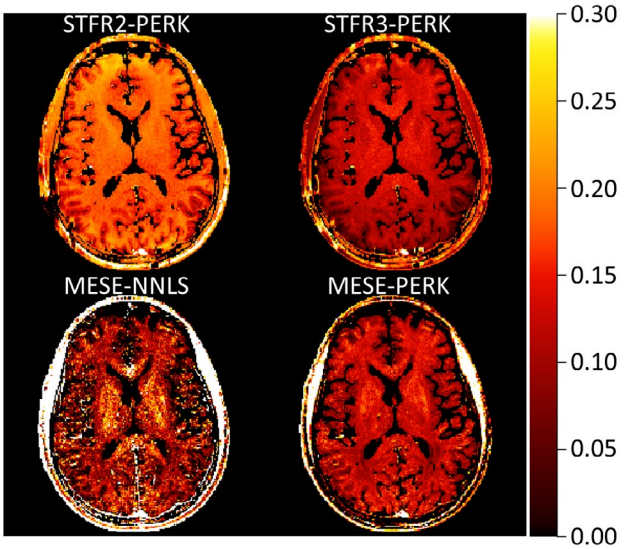

FIGURE 6 MWF maps from in vivo MESE data and STFR data using scan design A. Table 4 shows numerical results for several manually selected regions of interest. The MESE-NNLS MWF map appears noisier than those shown in other works. This is likely due to the lower SNR of our data due to differences in voxel size. To match the STFR resolution, we acquired MESE with 1.1 mm isotropic voxels, whereas often MESE data are collected with slice thickness of 5 mm and 1.6 mm or greater in the phase encode direction. Remarkably, MESE-PERK is much less noisy than MESE-NNLS. This is likely due to PERK being a Bayesian estimator that discourages estimates that are far from the mean MWF training value

constraint, and there is a wide spread of tip-up phases (see Table 2). This seems to suggest that most of the information needed for estimating MWF lies in the phase accrual that occurs between the tip-down and tip-up excitations, so the flip angles should be chosen to maximize SNR. Interestingly, however, an unreported experiment showed that a scan design with flip angles set to 15° and with an even spread of tip-up phases ϕ resulted in CRLBs that were many orders of magnitude worse than the optimized scans. This result emphasizes the importance of the scan design process in choosing scan parameters, because these optimized parameters are robust across a range of $\Delta\omega_f$ values (see Figure 2). We also looked at optimized scan parameters when fixing T_{free} to 6 ms. We found that the tip-up phases still covered a spread of values, but the range of phases was slightly smaller, which makes sense because a smaller T_{free} leads to less off-resonance precession.

The expected CRLB for scan design A is better than that of design B when compared across many values of the additional myelin water $\Delta\omega_f$ (see Figure 2), as expected because the optimization of design B ignored the presence of $\Delta\omega_f$. Figure 2 also illustrates the impact that $\Delta\omega_f$ has on estimates of MWF; MWF becomes harder to estimate as $\Delta\omega_f$ approaches 0. These findings appear to be at variance with the findings in,[39] where in multi-GRE MWF estimation modeling $\Delta\omega_f$ led to worse estimates at 3T. However, there is likely more information about $\Delta\omega_f$ in the STFR scans because of the optimized tip-up phases, which could explain why modeling $\Delta\omega_f$ in this work improved MWF estimation.

Simulated test data showed that scan design A and scan design B gave similarly good estimates of MWF across many values of $\Delta\omega_f$, at least for a range of tissue parameters (see Figure 3). At first glance, one may be surprised that design A performed noticeably better than design B with respect to the expected CRLB, and yet the 2 designs had similar RMSE values. One may also be surprised that the RMSE values were relatively small (about 25% of the mean MWF value) even though the expected CRLB predicted errors of 100% or more. However, PERK is a Bayesian estimator;

TABLE 4 Sample means ± SDs of MWF estimates for 4 white matter (WM) regions of interest (ROIs) and 1 gray matter (GM) ROI

ROI	STFR2-PERK	STFR3-PERK	MESE-NNLS	MESE-PERK
WM1	0.175 ± 0.021	0.116 ± 0.029	0.096 ± 0.042	0.105 ± 0.030
WM2	0.175 ± 0.009	0.117 ± 0.011	0.089 ± 0.046	0.097 ± 0.023
WM3	0.206 ± 0.010	0.133 ± 0.010	0.108 ± 0.036	0.133 ± 0.014
WM4	0.195 ± 0.008	0.138 ± 0.010	0.121 ± 0.039	0.141 ± 0.014
GM	0.187 ± 0.034	0.110 ± 0.029	0.034 ± 0.035	0.085 ± 0.034

Note: Figure 6 shows corresponding MWF maps, and Supporting Information Figure S1 shows the corresponding ROIs.

thus, the unbiased CRLB does not necessarily predict the precision of MWF estimates computed by PERK. We minimized the unbiased CRLB during scan design because of its simplicity, but recognize that other objective functions for scan optimization may be better suited for MWF estimates from PERK or other Bayesian estimation methods. We investigated the effect of bias in Section S3 of the Supporting Information.

Simulated test data also show that STFR-based myelin water imaging compares well to MESE-based approaches. Compared to the conventional MESE-NNLS, STFR3-PERK gives more accurate results in simulated WM voxels, in addition to reducing estimation time by more than an order of magnitude (see Table 3). This result is interesting because the simulated MESE echoes generally had much higher SNR than the STFR scans. Combining MESE with PERK improves upon the NNLS results. However, the MESE scan is longer than the combined time of all the STFR and BS scans. Furthermore, MWF estimation using MESE-PERK takes longer than STFR3-PERK because when simulating the MESE signal one must simulate a collection of spins to account for stimulated echoes, which is not necessary for STFR. This simulated data also show that ignoring exchange when estimating MWF with STFR scans results in drastically overestimated MWF values (see Figure 4), so it is essential to generate training data that account for exchange. These same results hold even when the test data were generated using a 9-compartment exchanging model (see Figure 5). See Section S2 of the Supporting Information for results using a 4-compartment exchanging model and a 3-compartment non-exchanging model.

The in vivo MWF estimates in Figure 6 further emphasize the importance of modeling exchange. The MWF map given by STFR2-PERK has higher MWF values than the map given by STFR3-PERK. The 3-compartment model led to maps that better agreed with the MWF maps estimated from MESE data. Table 4 indicates that in all WM ROIs the STFR3-PERK estimates are within 1 SD of the mean MESE-NNLS estimates. In GM it is different; however, this difference could be due to how the STFR training data were simulated, as typical values for GM $T_{1,f}$ and $T_{1,s}$ are slightly outside of the range of values generated for training. Figure 6 and Table 4 also demonstrate the effect that the estimation method has on MWF estimates: the MESE-PERK estimates have decreased SD compared to the MESE-NNLS estimates. Furthermore, Table 4 demonstrates that STFR-based MWF estimates have lower SD than MESE-based MWF estimates, despite the MESE scans being 4× longer than the STFR scans.

For the in vivo data, we did not use a separately acquired bulk off-resonance $\Delta\omega$ map as a known parameter for our proposed STFR-based MWF estimation technique, even though the scan design and simulations assumed that $\Delta\omega$ was known. When we attempted to use the separately acquired $\Delta\omega$ map for the in vivo data, the MWF estimates appeared to be more biased in regions with high $\Delta\omega$ values. Further work is needed to investigate this behavior.

For the in vivo data, we acquired a 9 mm slab in about 7 minutes total scan time with 1.1 mm isotropic resolution. Whole brain coverage would require 4 times as much data (with 2 mm slices), so our proposed approach would take about 28 minutes, which is longer than the 8 minutes achieved by the GRASE method. However, in[6] the authors under-sampled the GRASE data by a factor of 4, whereas we acquired fully sampled data. By under-sampling by the same factor the proposed STFR approach would achieve whole-brain coverage in about 7 minutes.

5 | CONCLUSION

This work optimized a set of STFR scans that can be used to estimate MWF. We found that estimates of MWF are more precise for larger values of the frequency difference $\Delta\omega_f$ between myelin water and non-myelin water. Fortunately, in WM reported values of $\Delta\omega_f$ are far enough away from 0 to aid estimation of MWF.[17] We also found that modeling exchange (ie, using a more accurate tissue model) greatly impacts the MWF estimates from STFR scans. When modeling exchange, STFR with PERK yields MWF estimates that are comparable to MESE-based MWF estimates.

This is the first work to compare STFR-based MWF estimation to MESE-based MWF estimation. Additionally, to our knowledge, this is the first work to generate MWF estimates from a MESE scan using PERK. While this estimation method was not the main point of this paper, it illustrates another potential method for MWF estimation.

This study was a proof-of-concept study to see if STFR could be applied to estimating MWF. As such, only a single healthy volunteer was scanned. While the initial comparison of STFR to MESE is promising, future studies should compare the 2 methods across multiple volunteers. Additionally, our proposed MWF estimation method should be validated in pathology to verify that it can detect, for example, multiple sclerosis lesions. Such verification is especially important because the proposed method assumes a fixed number of tissue compartments, which may or may not inhibit its sensitivity to anomalies.

There are several ways in which the scan design process could be further explored. Our choice to optimize 9 STFR scans for scan design was somewhat arbitrary, so one could explore different numbers of scans to see how the CRLB is affected for a given scan time budget. Additionally, one could change the space of scan parameters over which to optimize; especially interesting would be to increase the upper bound on α and β to see if the optimized scans would have a greater variety of flip angles. Another route to explore is to adjust the weighting matrix $\boldsymbol{W}$ to optimize STFR scans for estimating other parameters in addition to or instead of MWF. In particular, since the results here suggest that the STFR scans are sensitive to the effects of exchange, it could be interesting to optimize STFR scan design for quantifying exchange parameters. Additionally, future work could explore what parameters to include as known parameters versus unknown parameters, in both the scan design and in PERK.

Finally, to reduce the scan time of the STFR scans, either to allow for more scans or to reduce scan time, one could under-sample the MRI k-space data. The image reconstruction would then be under-determined, thus requiring some sort of regularized reconstruction. Methods that jointly reconstruct all D scans at once would be a natural approach (eg, Refs. 40,41).

ACKNOWLEDGMENTS

We thank Scott Swanson for discussions of exchange, and Mingjie Gao for discussions of scan optimization. We also thank Navid Seraji-Bozorgzad for discussion of in vivo results, and the reviewers for comments that improved the paper.

ORCID

Steven T. Whitaker http://orcid.org/0000-0003-1170-7653
Gopal Nataraj http://orcid.org/0000-0002-2847-115X
Jeffrey A. Fessler https://orcid.org/0000-0001-9998-3315

REFERENCES

1. Alonso-Ortiz E, Levesque IR, Pike GB. MRI-based myelin water imaging: a technical review. *Mag Res Med*. 2015;73:70–81.
2. West KL, Kelm ND, Carson RP, Gochberg DF, Ess KC, Does MD. Myelin volume fraction imaging with MRI. *Neuroimage*. 2018;182:511–521.
3. Mackay A, Whittall K, Adler J, Li D, Paty D, Graeb D. In vivo visualization of myelin water in brain by magnetic resonance. *Mag Res Med*. 1994;31:673–677.
4. Prasloski T, Rauscher A, MacKay AL, et al. Rapid whole cerebrum myelin water imaging using a 3D GRASE sequence. *NeuroImage*. 2012;63:533–539.
5. Prasloski T, Mädler B, Xiang QS, MacKay A, Jones C. Applications of stimulated echo correction to multicomponent T_2 analysis. *Mag Res Med*. 2012;67:1803–1814.
6. Zhang J, Vavasour I, Kolind S, Baumeister B, Rauscher A, MacKay AL. Advanced myelin water imaging techniques for rapid data acquisition and long T_2 component measurements. In Proceedings of the ISMRM, Milan, Italy, 2015. p. 824.
7. Deoni SCL, Rutt BK, Arun T, Pierpaoli C, Jones DK. Gleaning multicomponent T_1 and T_2 information from steady-state imaging data. *Mag Res Med*. 2008;60:1372–1387.
8. Zhang J, Kolind SH, Laule C, MacKay AL. Comparison of myelin water fraction from multiecho T_2 decay curve and steady-state methods. *Mag Res Med*. 2015;73:223–232.
9. West DJ, Teixeira RPAG, Wood TC, Hajnal JV, Tournier JD, Malik SJ. Inherent and unpredictable bias in multi-component DESPOT myelin water fraction estimation. *NeuroImage*. 2019;195:78–88.
10. Lankford CL, Does MD. On the inherent precision of mcDESPOT. *Mag Res Med*. 2013;69:127–136.
11. Hwang D, Kim DH, Du YP. In vivo multi-slice mapping of myelin water content using T_2* decay. *NeuroImage*. 2010;52:198–204.
12. Lenz C, Klarhöfer M, Scheffler K. Feasibility of in vivo myelin water imaging using 3D multigradient-echo pulse sequences. *Magn Reson Med*. 2012;68:523–528.
13. Nam Y, Lee J, Hwang D, Kim DH. Improved estimation of myelin water fraction using complex model fitting. *NeuroImage*. 2015;116:214–221.
14. Nataraj G, Nielsen JF, Fessler JA. Myelin water fraction estimation from optimized steady-state sequences using kernel ridge regression. In Proceedings of the ISMRM, Honolulu, Hawaii, USA, 2017. p. 5076.
15. Nataraj G, Nielsen JF, Gao M, Fessler JA. Fast, precise myelin water quantification using DESS MRI and kernel learning; 2018. http://arxiv.org/abs/1809.08908
16. Nataraj G, Gao M, Nielsen JF, Fessler JA. Kernel regression for fast myelin water imaging. In ISMRM Workshop on Machine Learning Part 2, Washington, DC, 2018. Vol. 2, 65.
17. Miller KL, Smith SM, Jezzard P. Asymmetries of the balanced SSFP profile. Part II: white matter. *Mag Res Med*. 2010;63:396–406.
18. Whitaker ST, Nataraj G, Gao M, Nielsen JF, Fessler JA. Myelin water fraction estimation using small-tip fast recovery MRI. In Proceedings of the ISMRM, Montreal, Canada, 2019. p. 4403.
19. Nielsen JF, Yoon D, Noll DC. Small-tip fast recovery imaging using non-slice-selective tailored tip-up pulses and radio frequency-spoiling. *Mag Res Med*. 2013;69:657–666.
20. Harkins KD, Dula AN, Does MD. Effect of intercompartmental water exchange on the apparent myelin water fraction in multi-exponential T_2 measurements of rat spinal cord. *Mag Res Med*. 2012;67:793–800.
21. Stanisz GJ, Kecojevic A, Bronskill MJ, Henkelman RM. Characterizing white matter with magnetization transfer and T_2. *Mag Res Med*. 1999;42:1128–1136.

22. Nataraj G, Nielsen JF, Scott CD, Fessler JA. Dictionary-free MRI PERK: parameter estimation via regression with kernels. *IEEE Trans Med Imaging*. 2018;37:2103–2114.
23. Sun H, Fessler JA, Noll DC, Nielsen JF. Steady-state functional MRI using spoiled small-tip fast recovery (STFR) imaging. *Mag Res Med*. 2015;73:536–543.
24. McConnell HM. Reaction rates by nuclear magnetic resonance. *J Chem Phys*. 1958;28:430–431.
25. Carr HY, Purcell EM. Effects of diffusion on free precession in nuclear magnetic resonance experiments. *Phys Rev*. 1954;94:630–638.
26. Hennig J. Multiecho imaging sequences with low refocusing flip angles. *J Mag Res*. 1988;88:397–407.
27. McGibney G, Smith MR. An unbiased signal-to-noise ratio measure for magnetic resonance images. *Med Phys*. 1993;20:1077–1078.
28. Nataraj G, Nielsen JF, Fessler JA. Optimizing MR scan design for model-based T_1, T_2 estimation from steady-state sequences. *IEEE Trans Med Imaging*. 2017;36:467–477.
29. Kay SM. *Fundamentals of statistical signal processing: estimation theory*. New York, NY: Prentice-Hall; 1993.
30. Jones JA, Hodgkinson P, Barker AL, Hore PJ. Optimal sampling strategies for the measurement of spin-spin relaxation times. *J Mag Res B*. 1996;113:25–34.
31. Voigt T, Nehrke K, Doessel O, Katscher U. T_1 corrected B_1 mapping using multi-TR gradient echo sequences. *Mag Res Med*. 2010;64:725–733.
32. Asslander J, Lattanzi R, Sodickson DK, Cloos MA. Optimized quantification of spin relaxation times in the hybrid state. *Mag Res Med*. 2019;82:1385–1397.
33. Nataraj G. *Advances in quantitative MRI: acquisition, estimation, and application* [PhD thesis]. Ann Arbor, MI: University of Michigan, 2018;48109–2122.
34. Rahimi A, Recht B. Random features for large-scale kernel machines. In: NIPS; 2007:1177–1184.
35. Deoni SCL. Correction of main and transmit magnetic field (B_0 and B_1) inhomogeneity effects in multicomponent-driven equilibrium single-pulse observation of T_1 and T_2. *Mag Res Med*. 2011;65:1021–1035.
36. Sacolick LI, Wiesinger F, Hancu I, Vogel MW. B_1 mapping by Bloch-Siegert shift. *Mag Res Med*. 2010;63:1315–1322.
37. Nielsen JF, Noll DC. TOPPE: a framework for rapid prototyping of MR pulse sequences. *Magn Reson Med*. 2018;79:3128–3134.
38. Collins DL, Zijdenbos AP, Kollokian V, et al. Design and construction of a realistic digital brain phantom. *IEEE Trans Med Imaging*. 1998;17:463–468.
39. Alonso-Ortiz E, Levesque IR, Pike GB. Impact of magnetic susceptibility anisotropy at 3 T and 7 T on T_2*-based myelin water fraction imaging. *NeuroImage*. 2018;182:370–378.
40. Mandava S, Keerthivasan MB, Li Z, Martin DR, Altbach MI, Bilgin A. Accelerated MR parameter mapping with a union of local subspaces constraint. *Mag Res Med*. 2018;80:2744–2758.
41. Wang X, Roeloffs V, Klosowski J, et al. Model-based T_1 mapping with sparsity constraints using single-shot inversion-recovery radial FLASH. *Mag Res Med*. 2018;79:730–740.

SUPPORTING INFORMATION

Additional Supporting Information may be found online in the Supporting Information section.

FIGURE S1 White matter (WM) and gray matter (GM) regions of interest (ROIs). The underlying image is from a standard MP-RAGE acquisition, acquired in the same scan session and registered to the other scans. The ROIs are labeled to correspond to Table 4 in the paper

FIGURE S2 RMSE of MWF estimates for WM and GM simulated test data. Scan design A has better RMSE in WM for values of $\Delta\omega_f$ we expect to see in WM. This better RMSE in WM is at the cost of worse RMSE in GM. Note that the values of $T_{1,f}$ and $T_{1,s}$ for GM were outside of the range of values used for the scan designs and for training our estimator

FIGURE S3 MWF maps from 5 methods using simulated test data for a 4-compartment tissue model with exchange. The 4 compartments considered were myelin water, axonal water (ie, water in myelinated axons), all other water, and macromolecules. The results are similar to those using the 3-compartment model with exchange. Supporting Information Table S1 shows numerical results

FIGURE S4 MWF maps from 5 methods using simulated test data for a 3-compartment tissue model without exchange. Without exchange, the 3-compartment model becomes essentially a 2-compartment model because the T_2 of the macromolecular pool is so small. Thus, it makes sense that STFR2-PERK performs well. Surprisingly, MESE-PERK still produces good MWF estimates, even though it is trained with the 3-compartment exchanging model (like STFR3-PERK). This could be because the T_R of the MESE scan is long compared to the residence times governing exchange. Furthermore, it is possible that if the training ranges for the residence times were adjusted appropriately (increased) then STFR3-PERK would also do well. Supporting Information Table S2 shows numerical results

FIGURE S5 In vivo images for 2 SPGR and 9 STFR scans using scan design A. Each image is the square root sum of squares combination of the individual coil data. STFR produces contrast similar to balanced SSFP, including a similar off-resonance profile that induces the characteristic banding artifact of balanced SSFP. Different points of this profile are sampled as the phase ϕ of the STFR tip-up excitation varies. The 9 STFR images are sorted by increasing ϕ, so this off-resonance profile is easily visualized. In the lower right is the field map estimated from the 2 SPGR scans

FIGURE S6 Comparison of biased and unbiased CRLBs for WM tissue values using the 2-compartment non-exchanging model. The biased CRLB is much lower than the unbiased CRLB, suggesting that bias is the reason why our STFR-based MWF estimation results in estimates with low variance. However, our proposed method still shows sensitivity to changes in MWF (see Supporting Information Figure S7)

FIGURE S7 Expected MWF estimates from the proposed STFR3-PERK MWF estimation technique for fixed WM tissue values from a 3-compartment exchanging model. The proposed method is (mildly) biased, yet it is still very sensitive to changes in true MWF value. Furthermore, bias decreases as SNR increases. (An unbiased estimator would have estimates along the line of identity, that is, along the dashed line)

TABLE S1 Numerical results for Supporting Information Figure S3

TABLE S2 Numerical results for Supporting Information Figure S4

How to cite this article: Whitaker ST, Nataraj G, Nielsen J-F, Fessler JA. Myelin water fraction estimation using small-tip fast recovery MRI. *Magn Reson Med*. 2020;84:1977–1990. https://doi.org/10.1002/mrm.28259

Supporting Information for Myelin Water Fraction Estimation Using Small-Tip Fast Recovery MRI

Steven T. Whitaker[1], Gopal Nataraj[2], Jon-Fredrik Nielsen[3], and Jeffrey A. Fessler[1]

[1]Department of Electrical Engineering and Computer Science, University of Michigan, Ann Arbor, Michigan, USA
[2]Department of Medical Physics, Memorial Sloan Kettering Cancer Center, New York, New York, USA
[3]Department of Biomedical Engineering, University of Michigan, Ann Arbor, Michigan, USA

This Supporting Information presents additional results and discussion for experiments not included in the main body of the manuscript.

S1 Estimator RMSE for White and Gray Matter Tissue Values

We compared MWF estimates from scan designs A and B. We simulated test data using the two-compartment non-exchanging STFR signal model using tissue values typical of white matter and gray matter (see Table 1), and we estimated MWF using STFR2-PERK. We plotted RMSE of MWF estimates from both scan designs versus the additional myelin water off-resonance $\Delta\omega_\mathrm{f}$. Supporting Information Figure S1 shows the results.

Supporting Information Figure S1 indicates that scan design A gives better MWF estimates in white matter over values of $\Delta\omega_\mathrm{f}$ we expect to see, but scan design B performs better in gray matter. However, the values of $T_{1,\mathrm{f}}$ and $T_{1,\mathrm{s}}$ for gray matter are (slightly) outside of the range of values used for the scan designs and for training our estimator. When quantifying MWF in gray matter is of interest, one probably should use a wider range of values for scan design and training.

S2 Estimator Performance with Model Mismatch

We compared MWF estimates from STFR2-PERK, STFR3-PERK, MESE-NNLS, MESE-PERK, and STFR3-PERK-JE for different ground truth models. First, we generated test data for white matter and gray matter tissue values using a four-compartment exchanging model. The four compartments were myelin water, axonal water (i.e., water in myelinated axons), all other water, and macromolecules. Myelin water was in exchange with the macromolecular pool, myelin water and axonal water exchanged with each other, and myelin water and all other water exchanged with each other. Supporting Information Figure S2 shows the results, and Supporting Information Table S1 reports numerical values. STFR3-PERK still provides good MWF estimates despite the model mismatch between the test data and the training data.

We then generated test data for white matter and gray matter tissue values using a three-compartment non-exchanging model. The three compartments were the same as in the three-compartment exchanging model that STFR3-PERK was trained with, except no exchange occurred (i.e., the exchange rates were set to 0). Supporting Information Figure S3 shows the results, and Supporting Information Table S2 reports numerical values. Without exchange, the three-compartment model becomes essentially a two-compartment model because the T_2 of the macromolecular pool is so small. Thus it makes sense that STFR2-PERK gives good MWF estimates. The overestimation of MWF could be because the macromolecular pool has a nonzero f_m, but since it contributes no signal the estimator assumes that the smaller signal is due to a larger MWF. MESE-NNLS does better without exchange, though it still underestimates gray matter MWF, while STFR3-PERK does poorly. It is possible, though, that if the training ranges for the residence times

Supporting Information Figure S1: White matter (WM) and gray matter (GM) regions of interest (ROIs). The underlying image is from a standard MP-RAGE acquisition, acquired in the same scan session and registered to the other scans. The ROIs are labeled to correspond to Table 4 in the paper.

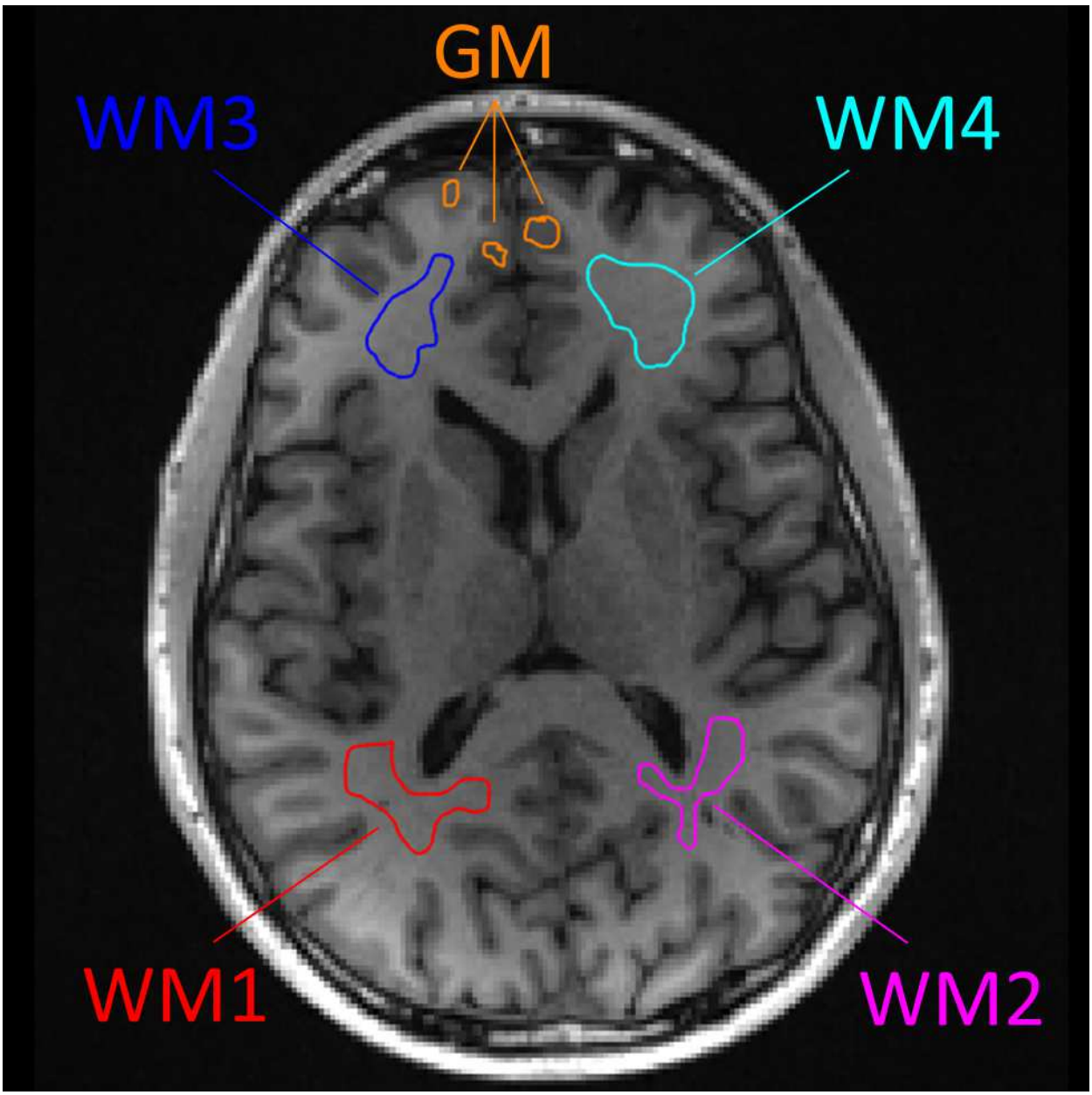

Supporting Information Table S1: Numerical results for Supporting Information Figure S2.

	White Matter (MWF = 0.15)			Gray Matter (MWF = 0.03)			
	RMSE	Mean	St. Dev.	RMSE	Mean	St. Dev.	Time (s)
STFR2-PERK	0.170	0.308	0.062	0.112	0.133	0.044	**14.7**
STFR3-PERK	**0.028**	**0.130**	**0.020**	**0.028**	0.052	0.017	42.1
STFR3-PERK-JE	0.040	0.120	0.026	**0.028**	**0.046**	0.022	42.2
MESE-NNLS	0.071	0.084	0.024	0.029	0.001	**0.004**	1623.6
MESE-PERK	0.033	0.127	0.023	0.056	-0.005	0.043	167.3

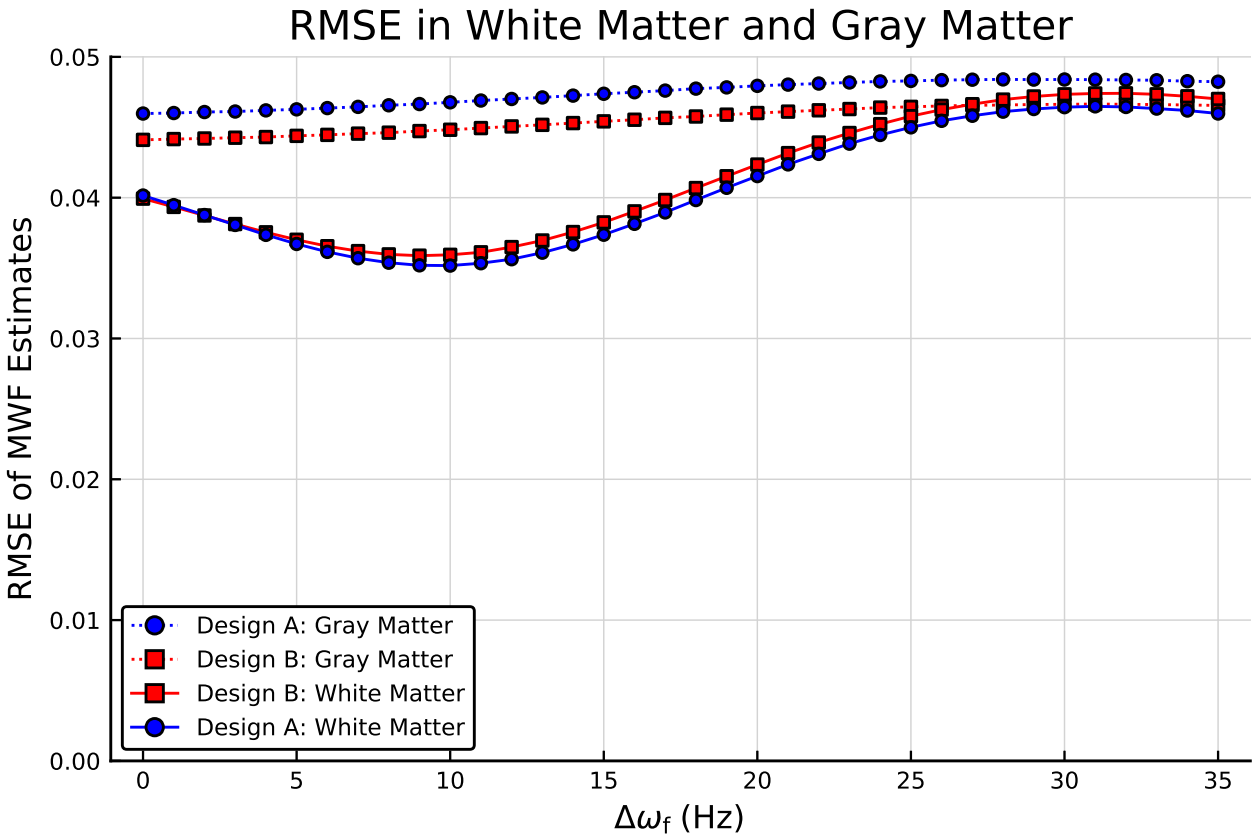

Supporting Information Figure S2: RMSE of MWF estimates for white matter and gray matter simulated test data. Scan design A has better RMSE in white matter for values of $\Delta\omega_{\mathrm{f}}$ we expect to see in white matter. This better RMSE in white matter is at the cost of worse RMSE in gray matter. Note that the values of $T_{1,\mathrm{f}}$ and $T_{1,\mathrm{s}}$ for gray matter were outside of the range of values used for the scan designs and for training our estimator.

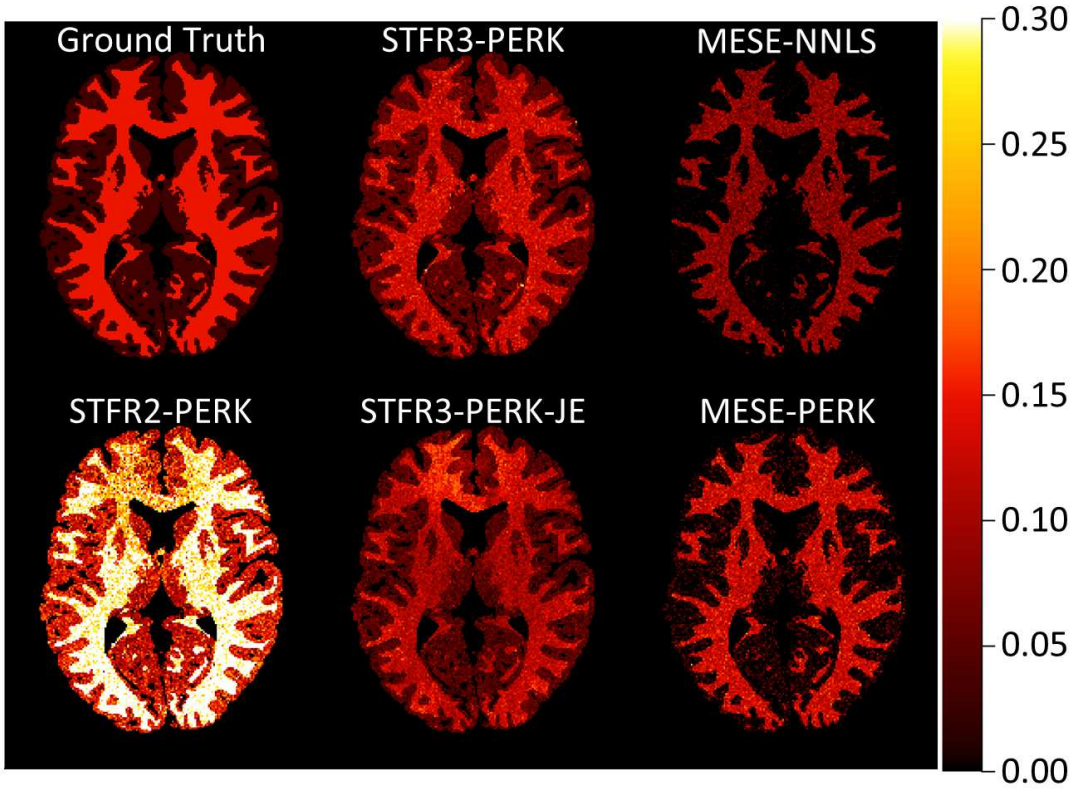

Supporting Information Figure S3: MWF maps from five methods using simulated test data for a four-compartment tissue model with exchange. The four compartments considered were myelin water, axonal water (i.e., water in myelinated axons), all other water, and macromolecules. The results are similar to those using the three-compartment model with exchange. Supporting Information Table S1 shows numerical results.

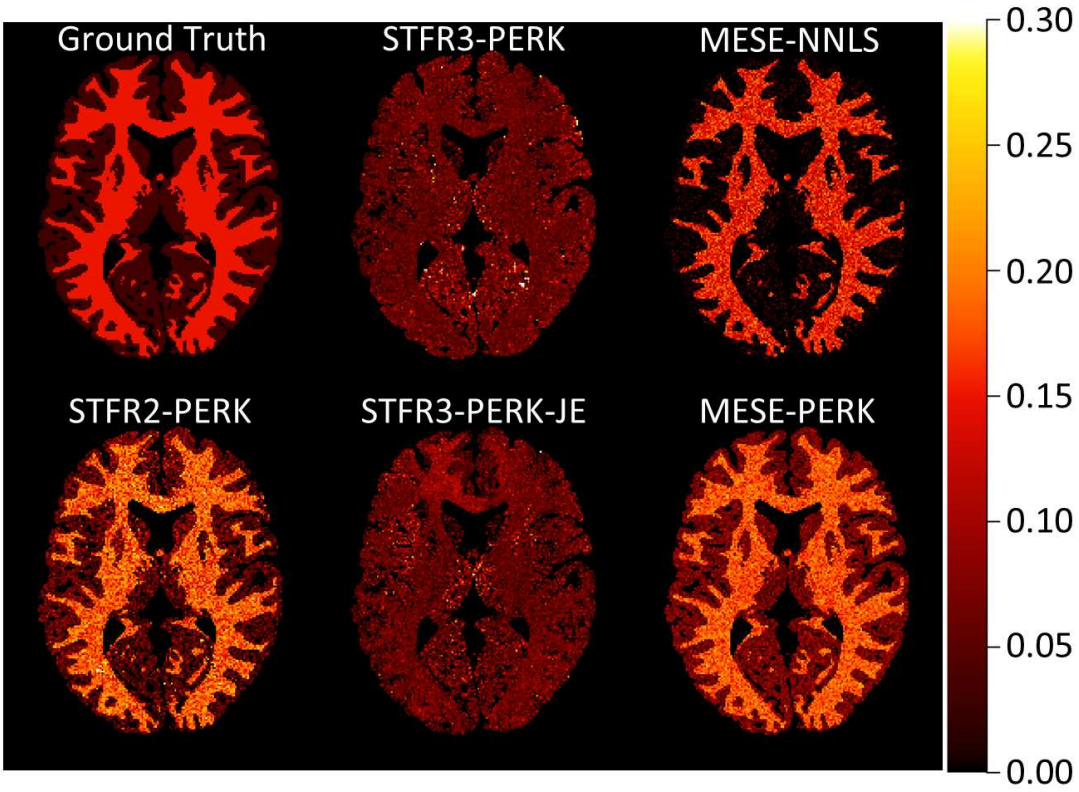

Supporting Information Figure S4: MWF maps from five methods using simulated test data for a three-compartment tissue model without exchange. Without exchange, the three-compartment model becomes essentially a two-compartment model because the T_2 of the macromolecular pool is so small. Thus it makes sense that STFR2-PERK performs well. Surprisingly, MESE-PERK still produces good MWF estimates, even though it is trained with the three-compartment exchanging model (like STFR3-PERK). This could be because the T_R of the MESE scan is long compared to the residence times governing exchange. Furthermore, it is possible that if the training ranges for the residence times were adjusted appropriately (increased) then STFR3-PERK would also do well. Supporting Information Table S2 shows numerical results.

were adjusted appropriately (increased, to allow for less exchange) then STFR3-PERK would also do well, although doing so might cause greater estimator bias. It is somewhat surprising that MESE-PERK still gives good MWF estimates, despite being trained with the three-compartment exchanging model. This could be because the T_R of the MESE scan is long compared to the residence times (more than 10× longer).

S3 Estimator Bias

To assess the effect of MWF estimator bias, we computed the biased CRLB [10] of scan design A for fixed white matter tissue values (for the two-compartment non-exchanging model). (This is unlike what we did in Figure 2, where we calculated an expected CRLB over distributions of the parameters.) The biased CRLB indeed was smaller than the unbiased CRLB (see Supporting Information Figure S5), suggesting that estimator bias is why our estimates had low variance. We investigated the bias of our STFR3-PERK estimator for test data using the three-compartment exchanging model with fixed white matter tissue values. We found that even with (mild) estimator bias, our proposed MWF estimation technique is still sensitive to changes in MWF (see Supporting Information Figure S6). Furthermore, our estimator bias decreases as SNR

Supporting Information Table S2: Numerical results for Supporting Information Figure S3.

	White Matter (MWF = 0.15)			Gray Matter (MWF = 0.03)			
	RMSE	Mean	St. Dev.	RMSE	Mean	St. Dev.	Time (s)
STFR2-PERK	0.048	0.181	0.037	0.047	**0.045**	0.044	**14.8**
STFR3-PERK	0.097	0.055	**0.020**	0.051	0.058	0.043	41.9
STFR3-PERK-JE	0.092	0.061	0.024	0.047	**0.045**	0.045	41.9
MESE-NNLS	**0.031**	**0.148**	0.031	**0.027**	0.007	**0.013**	1606.2
MESE-PERK	0.038	0.178	0.025	0.046	0.066	0.029	142.1

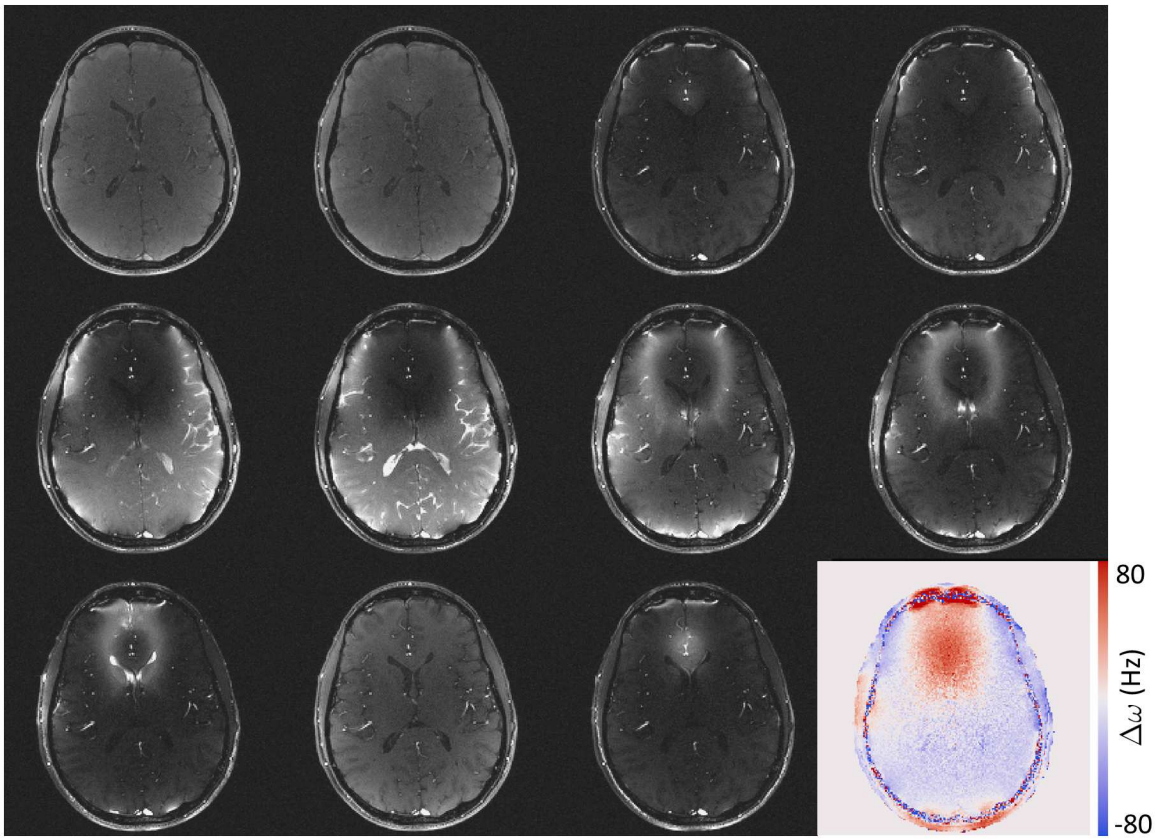

Supporting Information Figure S5: In vivo images for two SPGR and nine STFR scans using scan design A. Each image is the square root sum of squares combination of the individual coil data. STFR produces contrast similar to balanced SSFP, including a similar off-resonance profile that induces the characteristic banding artifact of balanced SSFP. Different points of this profile are sampled as the phase ϕ of the STFR tip-up excitation varies. The nine STFR images are sorted by increasing ϕ, so this off-resonance profile is easily visualized. In the lower right is the field map estimated from the two SPGR scans.

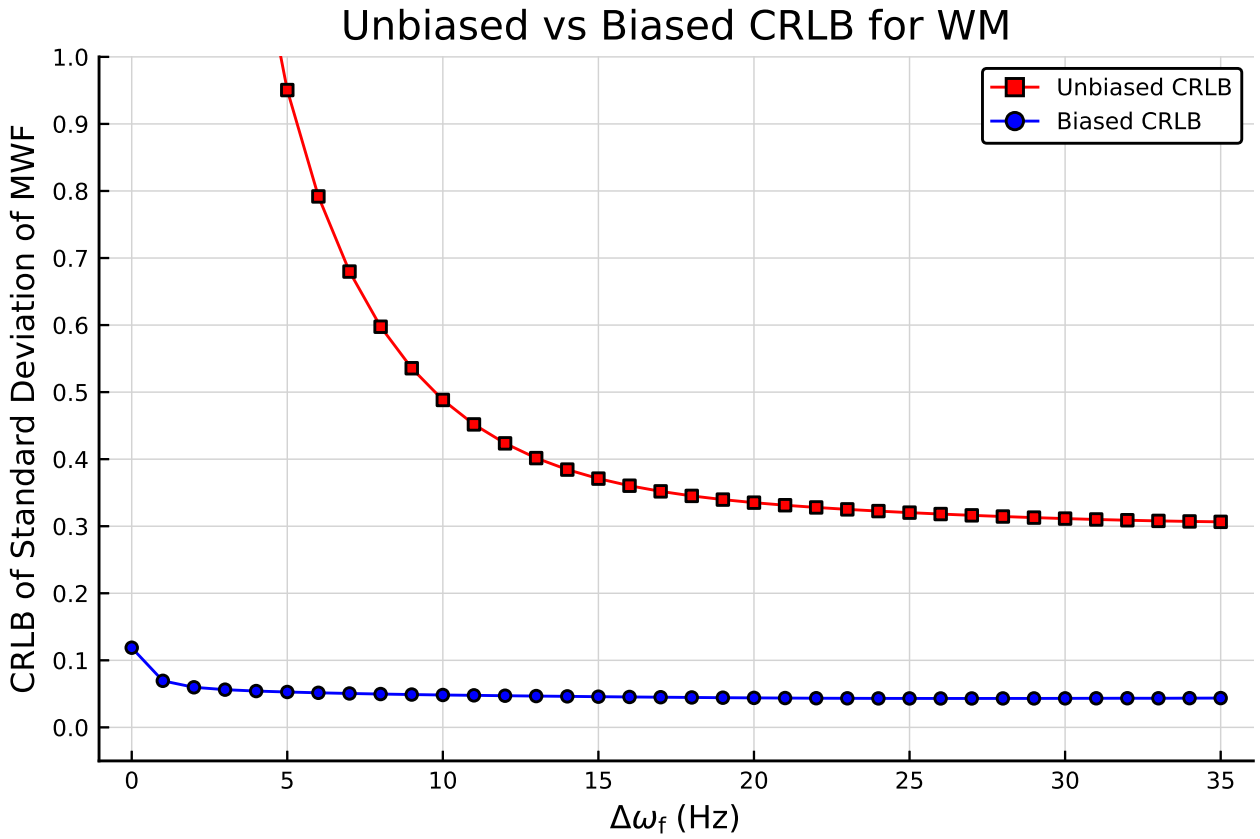

Supporting Information Figure S6: Comparison of biased and unbiased CRLBs for white matter tissue values using the two-compartment non-exchanging model. The biased CRLB is much lower than the unbiased CRLB, suggesting that bias is the reason why our STFR-based MWF estimation results in estimates with low variance. However, our proposed method still shows sensitivity to changes in MWF (see Supporting Information Figure S6).

increases (e.g., by using larger voxels). Thus, while the proposed method is biased, it still shows promise for detecting changes in MWF.

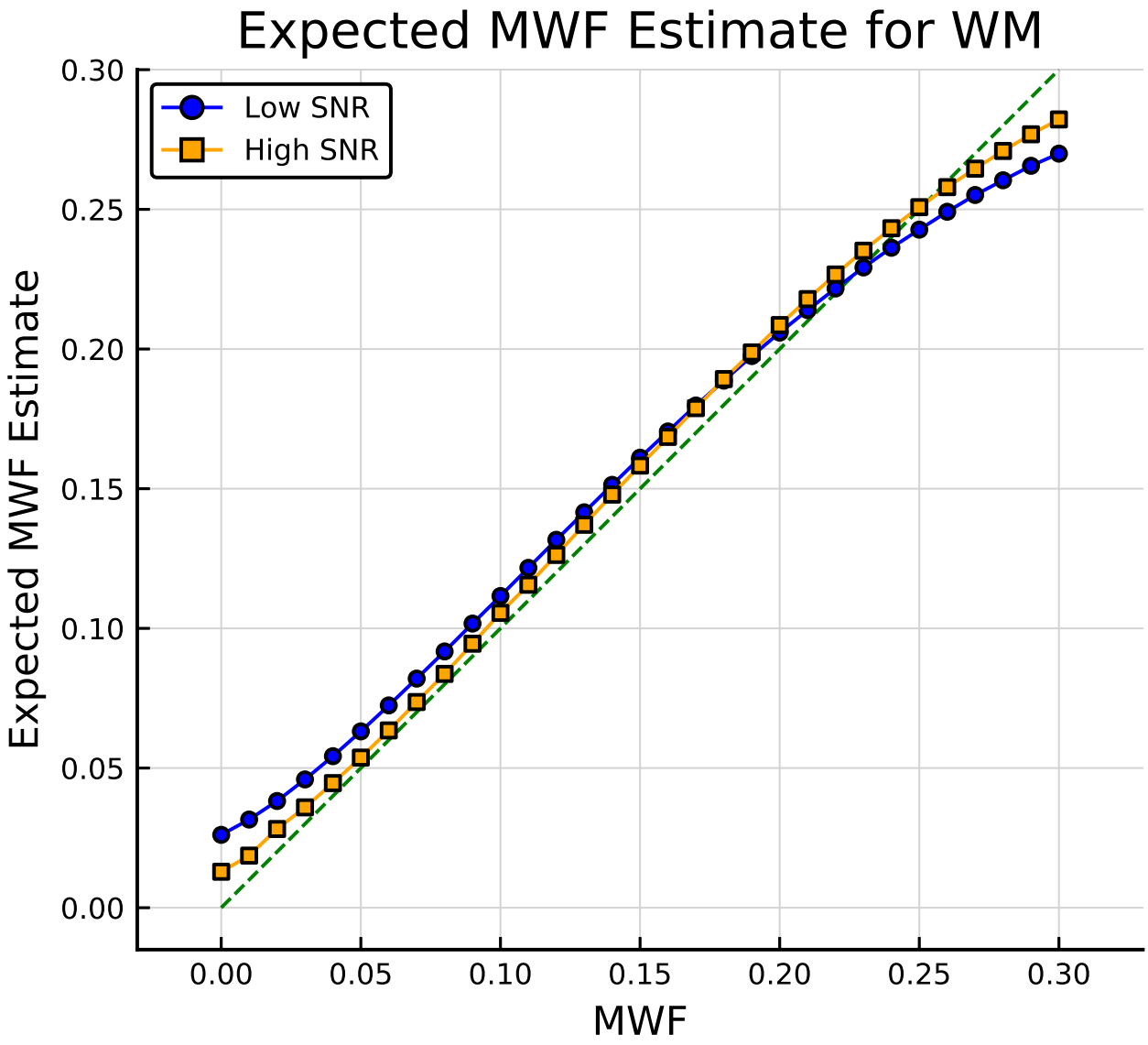

Supporting Information Figure S7: Expected MWF estimates from the proposed STFR3-PERK MWF estimation technique for fixed white matter tissue values from a three-compartment exchanging model. The proposed method is (mildly) biased, yet it is still very sensitive to changes in true MWF value. Furthermore, bias decreases as SNR increases. (An unbiased estimator would have estimates along the line of identity, i.e., along the dashed line.)